applied sciences

Article

Numerical Simulation Research on Aerodynamic Characteristics during Take-Off Phase in Ski Jumping

Qi Hu [1,2,*], Weidi Tang [1] and Yu Liu [1,*]

[1] School of Exercise and Health, Shanghai University of Sport, Shanghai 200438, China
[2] China Institute of Sport Science, Beijing 100061, China
* Correspondence: hqbuaa03@126.com (Q.H.); yuliu@sus.edu.cn (Y.L.)

Abstract: In view of the inability to directly and accurately obtain an athlete's aerodynamic force during the take-off phase through the wind tunnel test, the athlete's aerodynamic force and surrounding flow field form under different take-off postures are obtained through numerical simulation research, and the effects of different take-off modes on the aerodynamic characteristics during take-off in ski jumping are discussed. The multi-body system composed of the athlete and skis was selected as the research object. By using a partially averaged Navier–Stokes (PANS) turbulence model and a 3D numerical simulation of computational fluid dynamics (CFD), the aerodynamic characteristics of the athlete under different take-off postures were predicted. The take-off modes include the knee-push-hip (KPH) mode and hip-drive-knee (HDK) mode, and the hip joint angle of the HDK mode is significantly greater than that of the KPH mode. First, the aerodynamic force ratio of the athlete's torso and legs is obviously large. Although the aerodynamic forces of arms themselves are not obvious, they have a great impact on the overall aerodynamic characteristics of the athlete, so the posture of the arms cannot be ignored. The total drag and moment of the HDK mode are significantly higher than that of the KPH mode, and the lift-to-drag ratio of the HDK mode is significantly lower than that of the KPH mode. At first, the total lift of the HDK mode is higher than that of the KPH mode, but in the last attitude, the total lift of the HDK mode does not rise but fall, and finally, the total lift of the HDK mode is lower than that of the KPH mode. The aerodynamic characteristics change dramatically during the take-off phase, and the aerodynamic characteristics of the two take-off modes are quite different, and these changes and differences are difficult to observe during real training and at the competition site. The KPH mode has an obvious aerodynamic advantage over the HDK mode. During the take-off process, the athlete should increase the force generated by the knee joint extension and appropriately reduce the speed of the hip joint extension, control the using force order of the lower limb joints, and push the hip joint extension by the knee joint extension in order to avoid issues, such as the hip joint angle being too large, the hip joint extension angle being too fast, the center of gravity being too far back, and other problems. Studying the aerodynamic characteristics during the take-off phase provides valuable insights for athletes to achieve favorable flight postures after take-off, offering scientific guidance to improve their training strategies and enhance their competitive performance.

Keywords: aerodynamic characteristics; ski jumping; take-off; posture; computational fluid dynamics

check for updates

Citation: Hu, Q.; Tang, W.; Liu, Y. Numerical Simulation Research on Aerodynamic Characteristics during Take-Off Phase in Ski Jumping. *Appl. Sci.* **2024**, *14*, 1221. https://doi.org/10.3390/app14031221

Academic Editors: Enrique Navarro, Alejandro San Juan Ferrer and Santiago Veiga

Received: 27 December 2023
Revised: 23 January 2024
Accepted: 29 January 2024
Published: 1 February 2024

1. Introduction

Ski jumping is an exhilarating winter sports activity where athletes slide down a sloping ramp on specially designed skis. With the help of speed and the ground reaction force, they launch themselves into the air and land on a designated slope after a period of flight. The entire technique of ski jumping can be divided into four different phases: inrun, take-off, flight, and landing. These phases involve two major aspects: ballistics and aerodynamics. Ballistics depends on the athlete's speed and take-off position, while aerodynamics encompasses the aerodynamic characteristics of the anti-body system of the athlete and skis (such as the speed, athlete/ski system posture, drag and lift, clothing design, ski length, etc.) [1,2]. Both ballistics and aerodynamics pose specific requirements for ski jumpers, aiming to maximize vertical lift and minimize drag. Aerodynamics plays a crucial role in all four phases, although previous research has predominantly focused on the inrun and flight phases [3–6]. Computational fluid dynamics (CFD) is an important tool in the study of ski jumping aerodynamics as it allows for the direct and accurate calculation of an athlete's aerodynamic forces and moments. CFD can also provide visual or analytical representations of the surrounding flow field. However, the current CFD research on ski jumping is primarily focused on the inrun and flight stages [7–12]. The main reason for this is that, compared to the inrun and flight stages, the take-off stage involves rapid and drastic changes in the athlete's posture within a very short period. The dynamic complexity of this stage far exceeds that of the inrun and flight stages, making numerical simulation studies of the take-off process more challenging and less cost-effective.

The take-off phase is the transition motion from the inrun posture to the flight posture for ski jumpers. The take-off motion is considered to be the most important phase in the entire ski jumping performance because it plays a decisive role in the initial flight conditions [13]. During the take-off phase of ski jumping, the ballistic characteristics become more evident. Although some predictions have been made regarding its aerodynamic properties [14], the aerodynamic effects during the take-off phase have not been extensively studied. From an aerodynamic perspective, take-off is crucial because athletes need to strike a balance between maximizing vertical acceleration and minimizing aerodynamic drag. As the athlete extends their body to be fully exposed to the air during the take-off phase, the aerodynamic drag rapidly increases. However, the aerodynamic lift during the take-off phase is beneficial as it reduces the load on the athlete, leading to a shorter take-off time and a higher power development rate [15]. In actual ski jumping conditions, each jump training session is limited to a few seconds, and the take-off process itself lasts only about 0.3 s. However, a significant amount of time is required for preparation, and the number of training jumps completed per day is limited. Therefore, one effective way to improve an athlete's subjective perception of the aerodynamic forces and training duration is to conduct take-off training in a wind tunnel [16–19]. Furthermore, based on a series of wind tunnel experiments, Virmavirta et al. (2001) and Zhang et al. (2023) obtained force measurements by using the force measuring balance, which represents the combined effect of the take-off force and aerodynamic forces [15,20]. However, a direct measurement of the transient aerodynamic forces during take-off is still not possible. Additionally, by analyzing the kinematic parameters and take-off patterns of the top male ski jumpers in China, Tan et al. (2022) investigated the main factors influencing the flight distance in men's ski jumping [21]. Cao et al. (2022) found a correlation between the kinematic parameters of athletes during the take-off phase and the jumping distance, emphasizing the importance of powerful leg extension ability while utilizing speed and mastering the timing and direction of the take-off [22].

In summary, the research on the aerodynamic characteristics during the take-off phase of ski jumping mainly focuses on wind tunnel training and experimental testing, along with some analysis from a kinematic perspective. However, due to the rapid and significant changes in an athlete's postures during the take-off phase, and the limitations in the current level of experimental techniques in a wind tunnel, it is challenging to achieve consistent and stable reproductions of different take-off postures, and it is not possible to accurately test the aerodynamic forces and moments. Nevertheless, wind tunnel training can still be conducted to enhance athletes' subjective perception of the aerodynamic drag and their ability to adapt and adjust. To assist in improving the daily take-off and flight technique training for ski jumpers and accurately obtain the aerodynamic characteristics during the take-off phase, it is necessary to promptly initiate numerical simulation studies on the aerodynamic characteristics of the take-off phase in ski jumping. This will help in the investigation of the influence of athlete posture on the aerodynamic characteristics during the take-off phase, ultimately enabling athletes to achieve favorable flight postures after take-off. Considering the difficulties, complexity, and cost-effectiveness of conducting numerical simulations for the dynamic process during take-off, it is recommended that specific typical postures during take-off should be selected for static studies. This study aims to establish a detailed three-dimensional (3D) model and grid model of the athlete/ski system using the Partially Averaged Navier–Stokes (PANS) turbulence model for CFD numerical simulations. By doing so, the aerodynamic forces acting on the athletes and the flow field around them can be obtained for different take-off postures. This study will explore the impact of different take-off modes on the aerodynamic characteristics of ski jumpers.

2. Methodology

2.1. Research Subject

This research focuses on the multi-body system of ski jumpers and skis. To conduct targeted computational analyses and provide data support directly for national team training, this study conducts body posture scanning and data collection for an elite athlete in the national ski jumping team. The scan device combines phase and stereovision techniques to measure the three-dimensional surface of the human body. By projecting a grid pattern and capturing distorted images with two cameras, precise three-dimensional coordinates are obtained using coded light and phase-shifting methods. The 3D body scanning system utilizes optical scanning and harmless white light to rapidly capture comprehensive point cloud data of the human body. The resulting data offer accurate 3D information about various body parts, enabling precise body parameter measurements to be obtained with an overall accuracy of 0.5 mm.

By performing 3D scans of the athlete in different postures, a 3D-scanned model of the athlete's body during the inrun and take-off phases in ski jumping was obtained. Post-processing of the scanned point cloud data was conducted to obtain a closed 3D model representing the external contour of the athlete's body, which serves as the original model for CFD research, as shown in Figure 1. In the inrun and take-off phases of ski jumping, important posture parameters for the athlete include the ankle joint angle, φ1; knee joint angle, φ2; and hip joint angle, φ3.

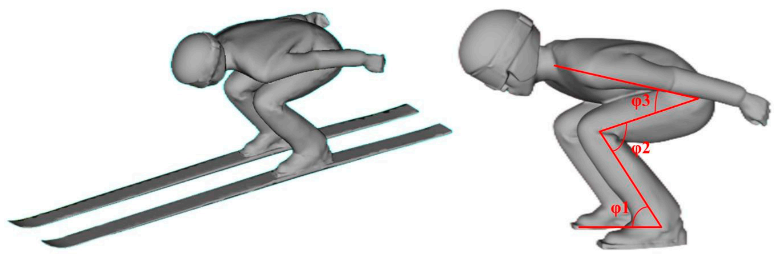

Figure 1. The original scanning model. φ1, ankle joint angle; φ2, knee joint angle; φ3, hip joint angle.

2.2. Research Methodology

2.2.1. Simulation Model

In this study, we utilize the large eddy simulation (LES) technique, which has been proven to be highly effective in numerically predicting flow separation around bluff bodies [4]. We choose LES over other methods because it offers several advantages, including the ability to better capture large-scale turbulent structures and the ability to resolve smaller scales without the need for excessive computational resources.

While the standard k-ε PANS model is widely used, it has certain limitations when simulating strong swirling flows and flows over highly curved surfaces. These limitations can lead to inaccurate predictions and compromises in the accuracy of the results. Therefore, we adopt the renormalization group (RNG) k-ε model, which has demonstrated improvements in simulating such flows [23].

The RNG k-ε model is selected based on its ability to handle complex flow phenomena more accurately. It incorporates the effects of turbulence anisotropy and non-equilibrium conditions, making it better suited for predicting flow characteristics in challenging scenarios. By using the RNG k-ε PANS turbulence model, we aim to enhance the accuracy of our simulations and obtain more reliable results.

By employing the RNG k-ε PANS turbulence model within the framework of the LES technique, we aim to overcome the limitations of previous models and capture the intricate flow features around bluff bodies with improved fidelity. This approach will lead to more accurate predictions and enhance our understanding of the flow physics involved, thereby contributing to advancements in the field of fluid dynamics.

To obtain more accurate results, the RNG k-ε PANS turbulence model is utilized, with its governing equations expressed as follows:

$$\frac{\partial(\rho k_u)}{\partial t} + \frac{\partial(\rho U_j k_u)}{\partial x_j} = \frac{\partial}{\partial x_j}\left[\alpha_k\left(\mu + \frac{\mu_u}{\sigma_u}\right)\frac{\partial k_u}{\partial x_j}\right] + P_{ku} - \rho\varepsilon_u \tag{1}$$

$$\frac{\partial(\rho\varepsilon_u)}{\partial t} + \frac{\partial(\rho U_j \varepsilon_u)}{\partial x_j} = \frac{\partial}{\partial x_j}\left[\alpha_k\left(\mu + \frac{\mu_u}{\sigma_u}\right)\frac{\partial \varepsilon_u}{\partial x_j}\right] + C^*_{\varepsilon 1} P_{ku}\frac{\varepsilon_u}{k_u} - C^*_{\varepsilon 2}\rho\frac{\varepsilon_u^2}{k_u} \tag{2}$$

In the equations, U_j represents the resolved velocity field, t denotes time, ρ represents fluid density, μ denotes the dynamic viscosity coefficient, μ_u represents the turbulent viscosity coefficient, f_k represents the unresolved turbulent kinetic energy ratio, f_ε represents the unresolved turbulent kinetic energy dissipation rate ratio, k_u represents the unresolved local time-averaged turbulent kinetic energy, and ε_u represents the unresolved local time-averaged turbulent kinetic energy dissipation rate, where

$$f_k = \frac{k_u}{k} \tag{3}$$

$$f_\varepsilon = \frac{\varepsilon_u}{\varepsilon} \tag{4}$$

$$\mu_u = \rho C_\mu \frac{k_u^2}{\varepsilon_u} \tag{5}$$

$$\sigma_u = \frac{f_k^2}{f_\varepsilon} \tag{6}$$

$$C^*_{\varepsilon 2} = C^*_{\varepsilon 1} + \frac{f_k}{f_\varepsilon}(C_{\varepsilon 2} - C^*_{\varepsilon 1}) \tag{7}$$

$$\eta = \left(2S_{ij} \cdot S_{ij}\right)^{1/2}\frac{k_u}{\varepsilon_u}\frac{f_\varepsilon}{f_k} \tag{8}$$

$$S_{ij} = \frac{1}{2}\left(\frac{\partial U_i}{\partial x_j} + \frac{\partial U_j}{\partial x_i}\right) \tag{9}$$

$$C^*_{\varepsilon 1} = C_{\varepsilon 1} - \frac{\eta(1 - \eta/\eta_0)}{1 + \delta\eta^3} \tag{10}$$

The values of the constants in the model are $C_\mu = 0.0845$, $\alpha_k = \alpha_\varepsilon = 1.39$, $C_{\varepsilon 1} = 1.42$, $C_{\varepsilon 2} = 1.68$, $\eta_0 = 4.377$, and $\delta = 0.012$.

The governing equations are discretized using the finite volume method. The coupling of pressure and velocity is solved using a consistent and coordinated approach based on the semi-implicit algorithm for pressure-linked equations (SIMPLEC). The time discretization is performed using a second-order difference scheme. The turbulent kinetic energy and velocity terms are discretized using a second-order upwind scheme. The time step size is set to 0.0001 s.

2.2.2. Validation of Model Independence from the Grid

The original 3D scan model of the research subject was adaptively modified, supplemented, and repaired based on the important parameters of the posture during the take-off phase. This process resulted in a refined 3D solid model of the multi-body system, allowing for the detailed modeling of the athlete's physical characteristics. Features such as fingers, ears, the face, shoulders, and hips can still be clearly distinguished from Figure 1.

The computational domain size for the ski jumper/skis multi-body system is 28 m in length, 11 m in width, and 14 m in height. Considering the presence of flow separation in the wake and the potential influence of the athlete's body shape on the flow field, the multi-body system's refined 3D solid model is divided into various regions for grid generation, as shown in Figure 2. These regions include the athlete's body surface area, the athlete's front region, the wake region behind the athlete's head and back, the wake region behind the athlete's waist and hips, the wake region behind the athlete's legs, the wake region behind the athlete's arms, and the region away from the athlete.

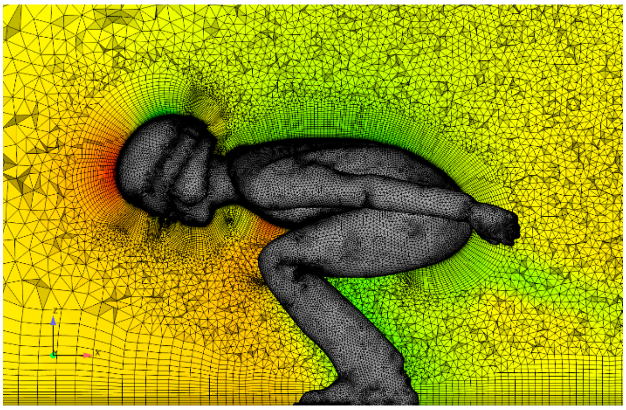

Figure 2. Grid distribution of the model surface and nearby area.

To meet the computational requirements of the RNG k-ε PANS model, an appropriate grid refinement strategy is applied around the athlete. The grid partitioning strategy used in this study has been previously validated in previous studies [4]. Specifically, for the grid model, four different grid densities are selected for each respective region. These regions are uniformly refined to varying degrees, resulting in grid point numbers ranging from 12.47 million to 23.21 million. The grid independence verification is conducted, and the results are presented in Table 1. The lift-to-drag ratios obtained from the last two grid validations are around 0.708. This shows that the computational domain discretization scheme with 20.03 million grid nodes can accurately predict its aerodynamic characteristics.

Table 1. Results of grid independency test.

	Grid Partitioning Strategy 1	Grid Partitioning Strategy 2	Grid Partitioning Strategy 3	Grid Partitioning Strategy 4
Total (gridmillion)	12.47	16.26	20.03	23.21
Lift-to-drag	0.749	0.715	0.708	0.708

2.2.3. Boundary Conditions and Computational Conditions

The boundary conditions were set as follows: (1) The inlet was specified as a velocity inlet, with a chosen inlet velocity of 25 m/s, representing the take-off speed in this study. (2) The outlet was set as a pressure outlet with a pressure value of 101,325 Pa, representing the atmospheric pressure. (3) The middle cross-section was assigned periodic boundary conditions. (4) The other walls were set as no-slip boundaries. (5) The fluid was assumed to be incompressible air. (6) The environment was subjected to a constant gravitational acceleration of g_0 = 9.807 m/s^2.

In this study, two take-off modes were considered: the knee-push-hip (KPH) mode and the hip-drive-knee (HDK) mode, with the hip joint angle being significantly greater in the HDK mode. The timing for the calculations started from the moment the front of the skis was about to leave the take-off ramp until the skis completely left the ramp, resulting in a total calculation time of approximately 90 ms. Throughout this process, six different postures of the athlete at different time intervals were selected for static computational conditions, as shown in Table 2. The CFD numerical simulations of the aerodynamic characteristics were conducted to analyze, under different take-off modes and postures, the forces and moments acting on the athlete and the flow field surrounding the athlete.

Table 2. Posture parameters and calculation conditions during take-off phase.

Time (ms)	φ1 (°)	φ2 (°)	φ3 (°)	
			KPH Mode	HDK Mode
−90	60	82	38	55
−72	64	93	47	81
−54	68	105	61	97
−36	72	115	75	109
−18	76	124	81	120
0	80	132	99	130

3. Results

3.1. Aerodynamic Forces and Moments

The aerodynamic forces acting on the multi-body system include lift and drag, and most of these forces do not act at the center of mass of the system, resulting in corresponding moments. Table 3 presents the mechanical characteristics of athletes in different postures under the two take-off modes. Figures 3–5 depict the variations in these characteristics over time. The forces listed in the results represent the resultant forces acting on various parts of the multi-body system, including the athlete and skis. The pitch moments listed in the results represent the moments relative to the midpoint of the line connecting the athlete's feet. The "+" symbol indicates that the moment causes the system to tilt backward, while "−" indicates that the moment causes the system to tilt forward. The lift-to-drag ratio in the results was calculated by dividing the lift by the drag.

Table 3. Results of aerodynamic characteristics of two take-off modes.

Time (ms)	Total Drag (N)		Total Lift (N)		Total Pitch Moment (N·m)		Lift-to-Drag Ratio	
	KPH Mode	HDK Mode	KPH Mode	HDK Mode	KPH Mode	HDK Mode	KPH Mode	HDK Mode
−90	40.20	50.66	31.31	35.56	19.69	28.06	0.779	0.702
−72	58.28	63.67	35.15	38.34	27.80	38.84	0.603	0.602
−54	65.27	76.91	39.26	42.91	35.14	52.42	0.601	0.558
−36	78.81	95.78	45.58	46.62	49.69	71.09	0.578	0.487
−18	86.78	119.90	50.79	55.45	57.47	85.31	0.585	0.462
0	99.05	140.01	53.58	51.09	69.05	98.82	0.541	0.365

In Figure 3a and Table 3, it can be observed that the total drag rapidly increases when the athlete's body becomes upright. Throughout the entire take-off process, the total drag in the KPH mode always remains significantly lower than that in the HDK mode. For the KPH mode, the initial total drag is 40.20 N, and the final total drag is 99.05 N, which is 2.46 times that of the initial value. For the HDK mode, the initial total drag is 50.66 N, and the final total drag is 140.01 N, which is 2.76 times that of the initial value. Although both take-off modes exhibit similar increasing trends in total drag, the growth rates differ slightly. In the case of the KPH mode, the total drag gradually increases at a nearly constant rate with a slight fluctuation during this phase. For the HDK mode, the total drag initially increases at a similar rate, and then the rise rate significantly increases in the last three postures.

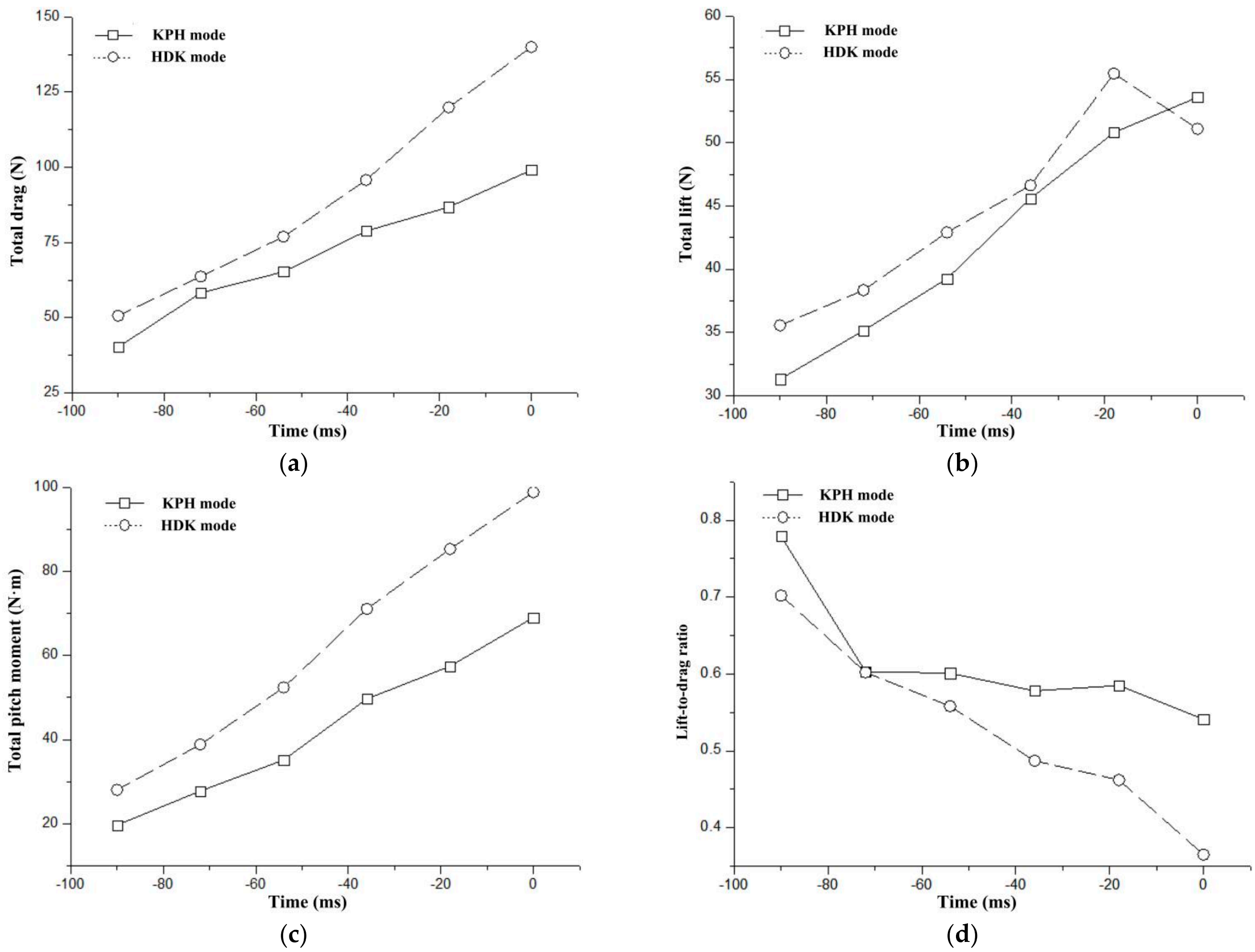

Figure 3. Change curves of aerodynamic characteristics of two take-off modes. Time −90 ms means the moment that the front of the skis is out of the platform. Time zero means the moment that the end of the skis completely leaves the platform. (**a**) The temporal changes in total drag. (**b**) The temporal changes in total lift. (**c**) The temporal changes in total pitch moment. (**d**) The temporal changes in lift-to-drag ratio.

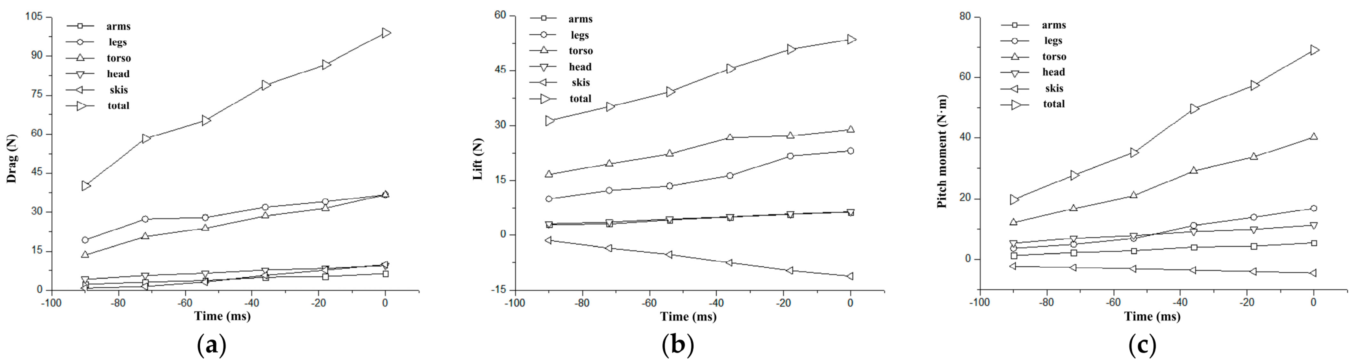

Figure 4. Change curves of different body parts' aerodynamic characteristics in KPH mode. (**a**) The temporal changes in drag, (**b**) the temporal changes in lift, and (**c**) the temporal changes in pitch moment.

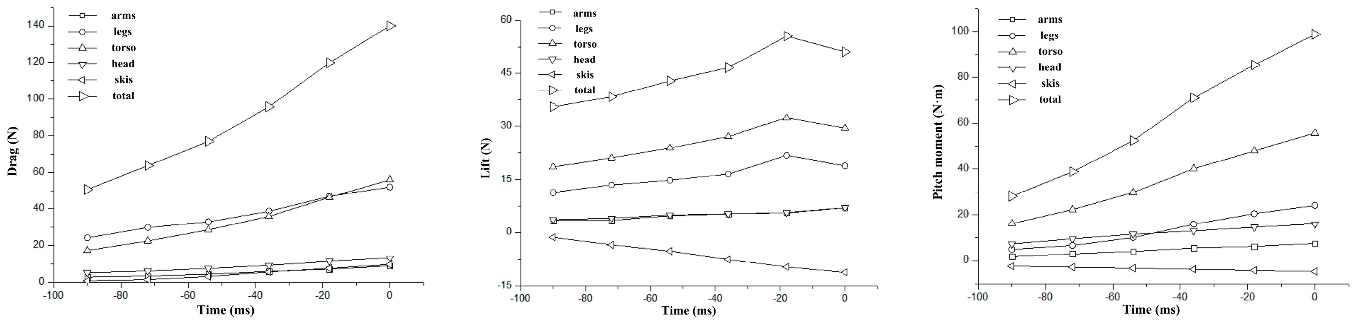

(**a**) (**b**) (**c**)

Figure 5. Change curves of different body parts' aerodynamic characteristics in HDK mode. (**a**) The temporal changes in drag. (**b**) The temporal changes in lift. (**c**) The temporal changes in pitch moment.

In Figure 3b and Table 3, it can be observed that in terms of the total lift, the KPH mode initially has a lower lift compared to the HDK mode. However, the total lift in the HDK mode steadily increases and reaches its peak at −18 ms but decreases slightly in the final posture. On the other hand, the total lift in the KPH mode steadily increases at a nearly constant rate. As a result, the final total lift in the KPH mode is higher than that in the HDK mode. For the KPH mode, the initial total lift is 31.31 N, and the final total lift is 53.58 N, which is 1.71 times that of the initial value. For the HDK mode, the initial total lift is 35.56 N, the lift peak is 55.54 N, and the final total lift is 51.09 N, with the lift peak being 1.56 times that of the initial value.

In Figure 3c and Table 3, it can be observed that the trend of the total pitch moment variation over time is similar to that of the total drag. The moment in the KPH mode steadily increases at a nearly constant rate, while the moment in the HDK mode experiences a significant rise rate increase in the latter half of the take-off. Throughout the entire take-off process, the moment in the KPH mode always remains significantly lower than that in the HDK mode. For the KPH mode, the initial moment is 19.69 N·m, and the final moment is 69.05 N·m, which is 3.51 times that of the initial value. For the HDK mode, the initial moment is 28.06 N·m, and the final moment is 98.82 N·m, which is 3.52 times that of the initial value.

From Figure 3d and Table 3, it can be observed that the change in the lift-to-drag ratio differs significantly between the two take-off modes, but the KPH mode consistently exhibits a higher lift-to-drag ratio than the HDK mode. For the KPH mode, the lift-to-drag ratio starts at 0.779 and decreases significantly, with some fluctuations around 0.6, and then decreases sharply. On the other hand, the lift-to-drag ratio in the HDK mode steadily decreases at a nearly constant rate. For the KPH mode, the lift-to-drag ratio decreases from 0.779 to 0.541, while for the HDK mode, it decreases from 0.702 to 0.365.

From Figures 4 and 5, it can be observed that for the drag characteristics, the athlete's torso and legs contribute the majority of the drag, with the torso's drag being slightly lower than that of the legs. Among the remaining parts, the head contributes a significant amount of drag, and the skis' contribution becomes more pronounced in the later stages when the skis experience an angle of attack, and it is almost comparable to that of the head. The arms and hands also contribute to the total drag, but to a lesser extent compared to the torso, legs, and head. For the lift characteristics, the athlete's torso and legs contribute the majority of the lift, with the torso's lift being generally higher than that of the legs. Among the remaining parts, the head and arms contribute almost the same lift, but the skis' lift is negative, and its absolute value steadily increases and then becomes higher than that of the head and arms in the later stages. In terms of the pitch moment characteristics, the athlete's torso contributes the majority of the moment. Among the remaining parts, the legs and head contribute more moment in turn, and the skis' moment is negative, and its absolute value is almost comparable to that of the head.

3.2. Flow Field Morphology

Figures 6 and 7 display the distribution of airflow velocity (i.e., the velocity component along the anterior–posterior direction) on the athlete's symmetry plane, also known as the sagittal plane. The regions of flow recirculation in the athlete's wake are highlighted in green or blue. These recirculation regions can be primarily divided into two distinct parts, with one part originating from the athlete's back and the other part originating from the athlete's chest. In certain postures, such as those in Figure 6c,d, the KPH mode exhibits slightly smaller recirculation regions. Additionally, it can be observed that there is an acceleration of airflow behind the head, in certain areas of the back and face, as well as between the athlete's legs. Conversely, there is a deceleration of airflow in the recirculation regions, in front of the athlete (face and chest), behind the neck, and below and behind the knees. The sizes of the low-velocity regions in the athlete's wake gradually increase over time, but in the HDK mode, these regions are significantly larger compared to the KPH mode, as shown in Figure 6e,f and Figure 7e,f. In the HDK mode, these low-velocity regions extend along the back in the last few postures, resulting in more deceleration of flow in front of the body.

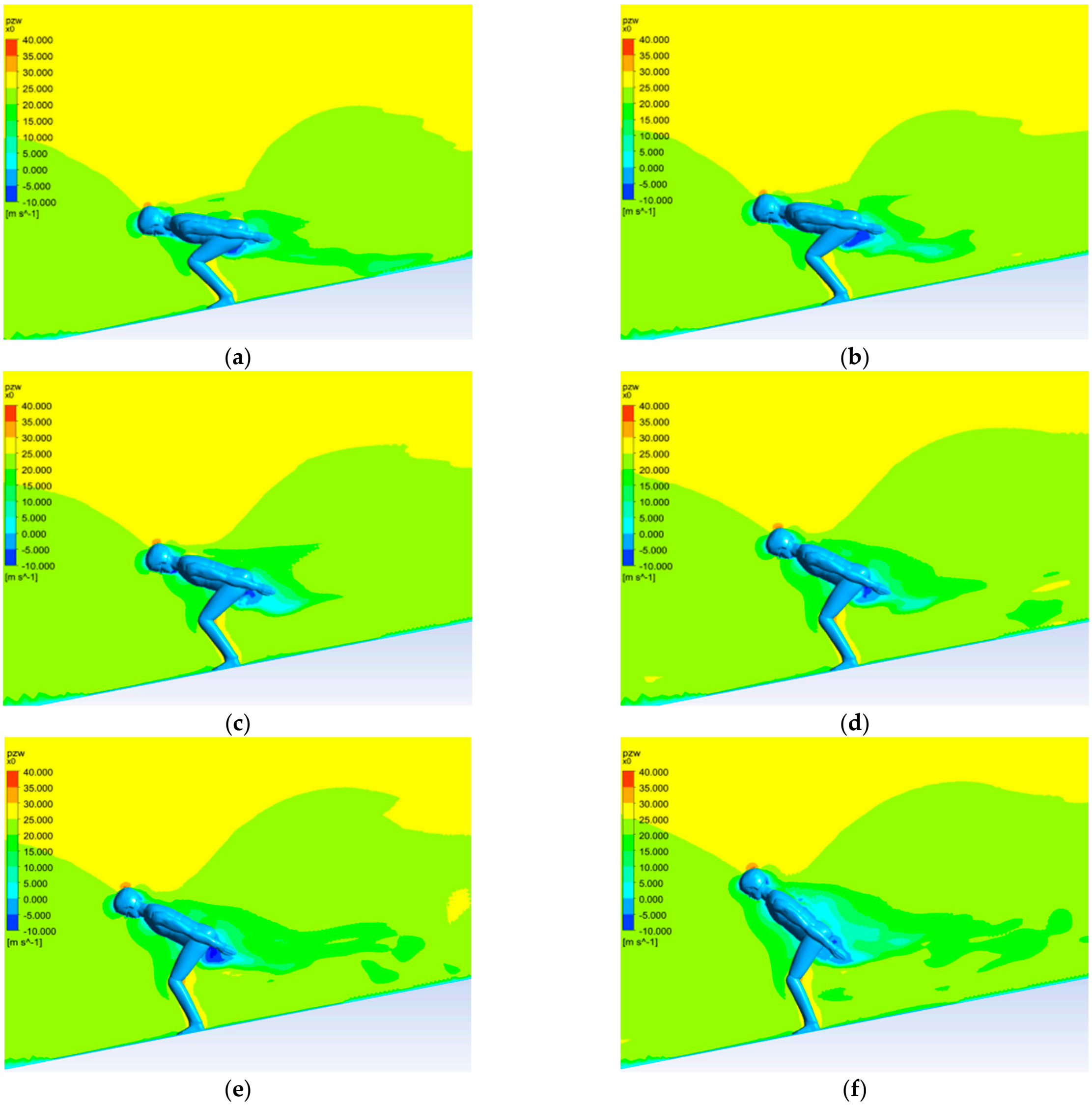

Figure 6. Airflow visualization of KPH mode. (**a**–**f**) The distribution of the average velocity, u, in the sagittal plane: (**a**) −90 ms, (**b**) −72 ms, (**c**) −54 ms, (**d**) −36 ms, (**e**) −18 ms, and (**f**) 0 ms.

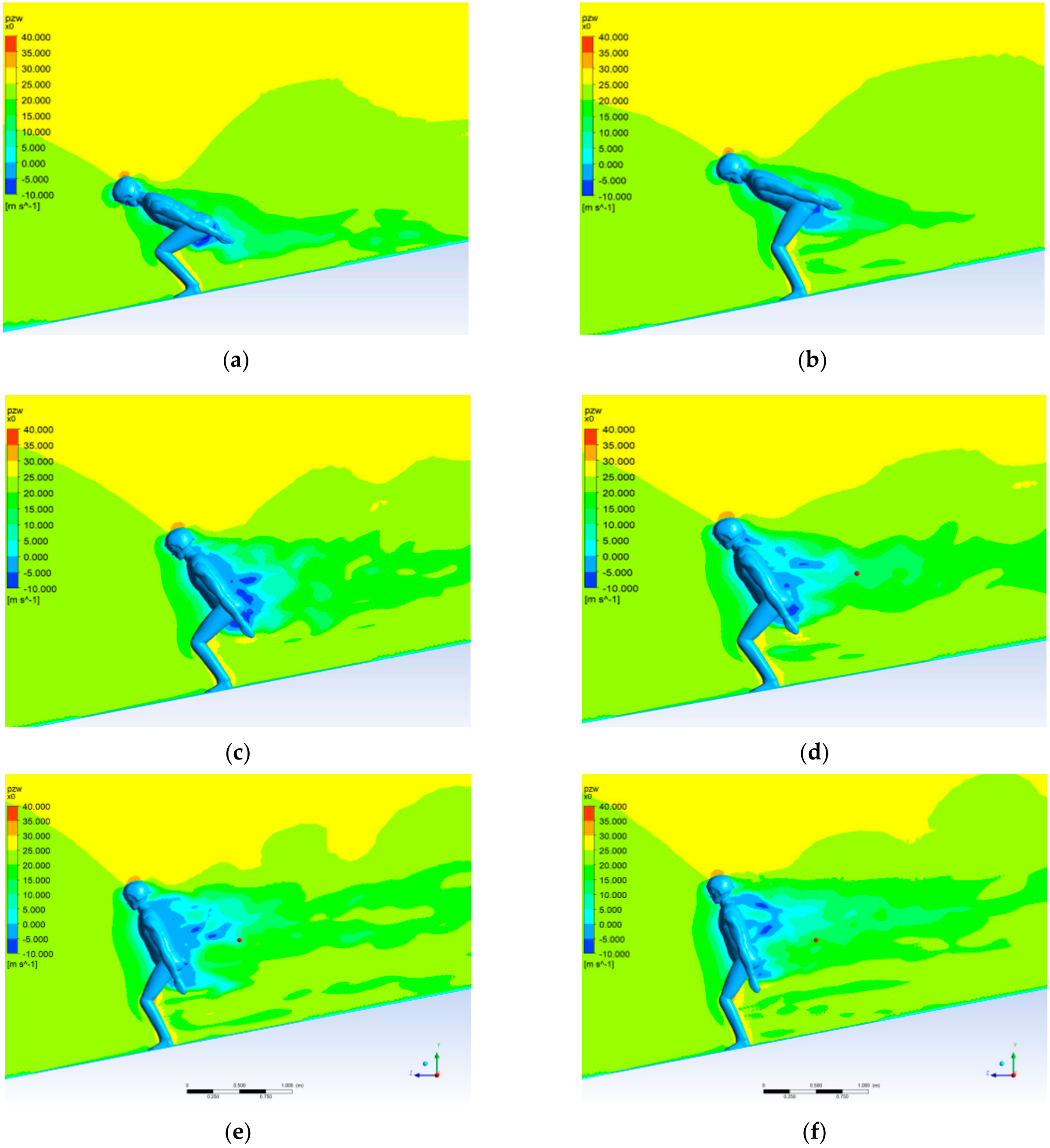

Figure 7. Airflow visualization of HDK mode. (a–f) The distribution of the average velocity, u, in the sagittal plane: (a) −90 ms, (b) −72 ms, (c) −54 ms, (d) −36 ms, (e) −18 ms, and (f) 0 ms.

Figure 8 illustrates the equal-vorticity contours (ω = 100 s^{-1}) observed from the side and back of the athlete. For the KPH mode, the vortices generated by the arms first separate and then tend to merge while gradually expanding downward. Throughout the entire take-off motion, these two distinct vortices are separated by a narrow vertical space and then generate a descending flow behind the athlete in the latter half of the take-off phase. However, for the HDK mode, these vortices combine with the vortices generated by the torso in the latter half of the take-off phase and transform into disordered vortices.

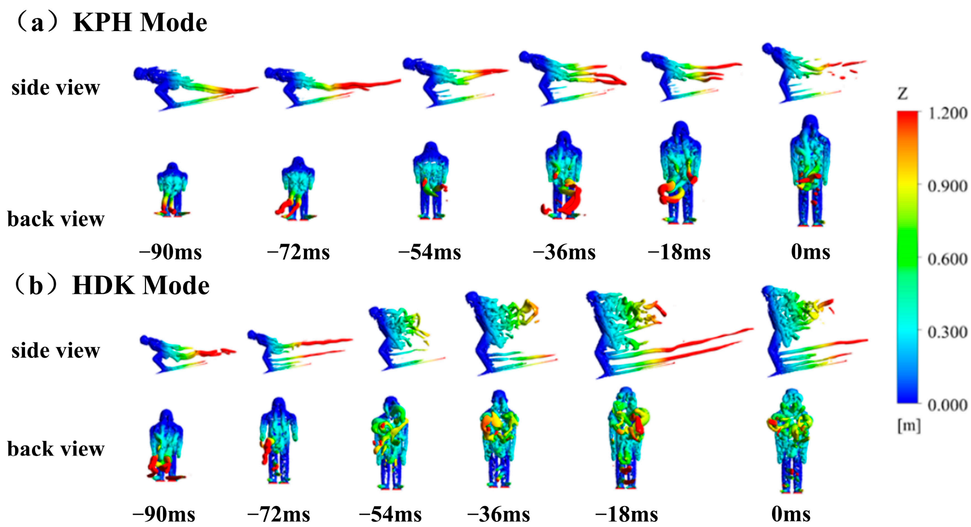

Figure 8. Comparison of the equal-vorticity contours of two take-off modes based on the side and back views. The equal vorticity contours (ω = 100 s^{-1}) were plotted. The colors indicate the anteroposterior distance from the surface.

4. Discussion

4.1. The Numerical Simulation Results' Validity Verification

In this study, the aerodynamic forces acting on the initial posture model during the take-off phase, which is the final posture model during the inrun phase, were found to be similar to the research results of Virmavirta et al. [15]. They conducted wind tunnel tests on athletes in the inrun phase posture under a wind speed of 27 m/s and measured the aerodynamic drag to range from 39.2 N to 59.7 N and aerodynamic lift ranging from 22.3 N to 50.4 N. In our study, the total drag for the initial posture in the KPH mode was 40.20 N, and in the HDK mode, it was 50.66 N. The total lift for the initial posture in the KPH mode was 31.31 N, and in the HDK mode, it was 35.56 N. The aerodynamic force results obtained in this study fall within the range of variability observed in wind tunnel tests. The comparison of these results validates the effectiveness of the CFD numerical simulation results and also indicates that even slight differences in the inrun and take-off postures have a significant impact on the aerodynamic characteristics.

4.2. Aerodynamic Characteristics of Different Body Parts

From Figures 4 and 5, it can be observed that the mechanical characteristics of different body parts of the athlete show similar variations over time for both take-off modes. Additionally, the mechanical characteristics of the skis have a relatively small impact but should not be ignored. The torso and legs of the athlete are the main contributors to aerodynamic forces, while the arms, head, and skis themselves also contribute, albeit to a lesser extent. In terms of the drag characteristics, the torso and legs contribute the majority of drag, accounting for approximately 80%. For the lift characteristics, the torso and legs also contribute the majority of lift, accounting for approximately 85%. Regarding the moment characteristics, the torso contributes the majority of the moment, accounting for over 57%, and the remaining significant contributors are the legs and head.

In the KPH mode, the double vortex flow generated by the arms creates a downwash vortex behind the athlete, as shown in Figure 8. This downwash vortex increases in circulation around the athlete, resulting in an increased lift effect, leading to a rapid increase in the total lift for the same period. In the HDK mode, in the initial take-off posture, the vortex flow from the arms is quite evident, but later on, these vortex flows become disordered (Figure 8, HDK mode, image of −54 ms). It can be inferred that these disordered vortex flows contribute to the increased area of low-speed regions in the wake of the HDK mode (Figure 7d), which subsequently leads to a decrease in the total lift

(Figure 3b). The study found that when the arm is in a low position, particularly in the HDK mode, it has a significant influence on the flow. This is because in the HDK mode, the arms are always very close to the athlete's thighs (Figure 7), generating larger disordered vortex flows during the entire take-off motion. These findings indicate that the vortices generated by the arms have a significant impact on the generation of aerodynamic lift and the flow structure behind the athlete. Although the aerodynamic forces generated by the arms themselves may not be significant, they have a substantial influence on the overall aerodynamic characteristics of the athlete. Meile et al. (2006) suggested considering the arm angle in flight phase postures and found that the aerodynamic lift during the flight phase increases with an increase in the shoulder joint abduction angle [12]. Additionally, Keizo, in his CFD study on ski jumping in the inrun and take-off phase, found that the positioning of the athlete's arms should not be ignored, as elite athletes are able to control the impact of their arms within a smaller range [24].

4.3. Aerodynamic Characteristics of Different Take-Off Postures

It can be observed that the HDK mode exhibits a significantly higher total drag compared to the KPH mode. This is mainly due to the difference in hip joint angles, or the angle of attack of the torso. As shown in Figures 6 and 7, the angle of attack of the torso is noticeably higher in the HDK mode compared to the KPH mode. Figure 7e clearly shows a large area of a low-speed region behind the athlete in the HDK mode at −18 ms. This low-speed region represents a decrease or even stagnation in the airflow velocity, and its size is an important factor influencing the pressure drag acting upon the athlete. The separation of airflow behind the athlete is caused by the excessive upright posture of the torso, resulting in the formation of this low-speed region and subsequently increasing the pressure drag acting upon the athlete.

Although the HDK mode initially exhibits a higher total lift compared to the KPH mode, in the final take-off posture, the total lift in the HDK mode does not continue to increase but decreases. This results in a reversal of the lift values at the last time stage (Figure 3b). It can be considered that the HDK mode experiences a stall phenomenon at the last time stage, where an increase in the angle of attack leads to a decrease in the lift coefficient. Virmavirta et al. (2001) suggested that a good take-off helps the athlete achieve a favorable flight posture, specifically a forward-leaning position, during the early flight phase [15]. Additionally, Schmölzer and Müller (2002) proposed that the aerodynamic lift should gradually increase during the early flight phase after the take-off phase [25]. Therefore, when a stall occurs in the HDK mode, it can put the athlete's aerodynamic characteristics in a disadvantageous state during the flight phase.

In Figure 3a,c, it is evident that the moment trends over time are similar to the total drag trend. In this study, the moment refers to the pitch moment, with "+" representing a moment that causes the multi-body system, i.e., the athlete, to tilt backwards, and "−" representing a moment that causes the multi-body system to tilt forwards. Schwameder (2008) suggested that one of the main objectives in the take-off phase is for the athlete to acquire angular momentum for forward rotation [26]. To achieve a favorable flight posture, for the HDK mode, the athlete must consume more physical energy to generate more forward rotational angular momentum compared to the KPH mode, as the aerodynamic forces generate a larger pitch moment, which causes the athlete to tilt backwards in the HDK mode compared to the KPH mode, as shown in Figure 3c.

In Figure 3d, it is evident that the lift-to-drag ratio of the KPH mode is consistently higher than that of the HDK mode. From the aerodynamic perspective, this is because the body opening angle in the KPH mode is significantly smaller than that in the HDK mode. The KPH mode provides a noticeable aerodynamic advantage for the athlete in the flight phase after the take-off phase. During the take-off process, to create favorable aerodynamic conditions for the early flight phase, the athlete should increase the force generated by the knee joint extension and appropriately reduce the speed of the hip joint extension, control the using force order of the lower limb joints, and push the hip joint extension by the knee joint extension in order to avoid issues such as the hip joint angle being too large, the hip joint extension angle being too fast, the center of gravity being too far back, and other problems, and to avoid the adverse impact of aerodynamic drag on take-off. Cao et al. (2022) demonstrated in their study on Chinese male ski jumpers that athletes should lower their center of gravity as much as possible while maximizing the utilization of speed at the start of the take-off phase to reduce drag, increase the knee joint extension force during the take-off phase, and simultaneously appropriately reduce the hip joint extension speed to avoid adverse effects of aerodynamic drag on the torso during the take-off phase [22]. They should also control the timing and direction of the take-off [21].

4.4. Limitations

The take-off phase in ski jumping is a dynamically complex process where the body posture continuously adjusts. Due to the technical limitations in studying its dynamic aspects, this research focused on analyzing selected static postures during take-off. However, this study did not consider the influence of the aerodynamic characteristics of ski jumping suits or the impact of changes in arm and head postures, particularly arm positioning, on the aerodynamic properties. These limitations highlight the need for further research to explore the complete dynamics and aerodynamic aspects of ski jumping, considering factors such as clothing design and body posture variations.

5. Conclusions

(1) Through numerical simulations using CFD, the aerodynamic characteristics and differences in various postures in the take-off phase in ski jumping have been analyzed. This study focuses on comparing the effects of two take-off modes on aerodynamic characteristics. The aerodynamic characteristics change dramatically during the take-off phase, and the aerodynamic characteristics of the two take-off modes are quite different, and these changes and differences are difficult to observe during real training and at the competition site.

(2) The aerodynamic forces on the athlete's torso and legs are significantly larger, while the contribution of the arms may be less pronounced. However, the position of the arms should not be ignored as it can still have a considerable impact on the overall aerodynamic characteristics of the athlete. The KPH mode demonstrates clear aerodynamic advantages. During the take-off process, the athlete should increase the force generated by the knee joint extension and appropriately reduce the speed of the hip joint extension, control the using force order of the lower limb joints, and push the hip joint extension by knee joint extension in order to avoid issues such as the hip joint angle being too large, the hip joint extension angle being too fast, the center of gravity being too far back, and other problems, and to avoid the adverse impact of the aerodynamic drag on take-off. This creates favorable aerodynamic conditions for the early flight phase.

(3) Numerical simulations of the aerodynamics in the take-off phase of ski jumping can accurately capture the aerodynamic characteristics. Numerical simulations combined with repeated training in a wind tunnel to simulate competition scenarios help athletes improve their subjective perceptions and adaptability to aerodynamic forces during the take-off phase. It also enables athletes to utilize aerodynamic forces to achieve favorable flight postures after the take-off phase. This research provides important scientific guidance for athletes to improve their take-off and flight technique training strategies and enhance their competitive performance.

(4) Computational fluid dynamics (CFD) techniques can be employed to model and simulate the flow of air around athletes, sports equipment, or sports facilities. These simulations can provide valuable insights into aerodynamic forces, drag, lift, and other relevant parameters, aiding in the design and optimization of sports equipment, training techniques, and performance analysis. CFD simulations can also help increase

understanding of the impact of wind conditions on sports performance, enabling athletes to make informed decisions and improve their strategies.

Author Contributions: Formal analysis, Q.H.; methodology, Q.H. and W.T.; writing—original draft, Q.H. and W.T.; writing—review and editing, Q.H., W.T., and Y.L.; funding acquisition, Q.H. and Y.L. All authors have read and agreed to the published version of the manuscript.

Funding: This research was funded by the National Key Research and Development Plan Project of China, grant number 2018YFF0300500, and the National Natural Science Foundation of China, grant numbers 11932013 and 11802068.

Institutional Review Board Statement: Not applicable.

Informed Consent Statement: Not applicable.

Data Availability Statement: The raw data supporting the conclusions of this article will be made available by the authors on request.

Acknowledgments: The authors would also like to express their gratitude to Chongli Wang and Qingli Li from the Aerodynaiviics Research Institute in China for conducting the 3D scanning of the athletes' postures and providing the original scanned models of the athletes.

Conflicts of Interest: The authors declare no conflicts of interest.

References

1. Hu, Q.; Liu, Y. A Review of Wind Tunnel Experimental Research on Aerodynamic Drag Reduction in Winter Sports. *China Sport Sci.* **2022**, *42*, 55–67.
2. Virmavirta, M. Aerodynamics of ski jumping. In *The Engineering Approach to Winter Sports*, 6th ed.; Braghin: New York, NY, USA, 2016; pp. 153–181.
3. Elfmark, O.; Ettema, G. Aerodynamic investigation of the inrun position in Ski jumping. *Sports Biomech.* **2021**, *19*, 1. [CrossRef]
4. Hu, Q.; Liu, Y. Effects of Athlete's Posture on Aerodynamic Characteristics during Flight in Ski Jumping. *J. Med. Biomech.* **2021**, *36*, 407–414.
5. Gardan, N.; Schneider, A.; Polidori, G.; Trenchard, H.; Seigneur, J.M.; Beaumont, F.; Fourchet, F.; Taiar, R. Numerical investigation of the early flight phase in ski-jumping. *J. Biomech.* **2017**, *50*, 29–34. [CrossRef]
6. Murakami, M.; Iwase, M.; Seo, K.; Ohgi, Y.; Koyanagi, R. High-speed video image analysis of ski jumping flight posture. *Sports Eng.* **2014**, *17*, 217–225. [CrossRef]
7. Tang, W.D.; Suo, X.; Yang, C.H.; Cao, F.R.; Wu, X.; Liu, Y. Computational Fluid Dynamics Simulation and Optimization of In-run Stage in Ski-Jumping. *China Sport Sci.* **2022**, *42*, 62–70.
8. Ryu, M.; Cho, L.; Cho, J. Aerodynamic analysis on postures of ski jumpers during flight using computational fluid dynamics. *Trans. Jpn. Soc. Aeronaut. Space Sci.* **2015**, *58*, 204–212. [CrossRef]
9. Chen, Z.F. Numerical Study of the Aerodynamical Parameters During the Flying Stage of Ski Jumping. *Zhejiang Sport Sci.* **2014**, *36*, 121–124.
10. Lee, K.D.; Park, M.J.; Kim, K.Y. Optimization of ski jumper's posture considering lift-to-drag ratio and stability. *J. Biomech.* **2012**, *45*, 2125–2132. [CrossRef] [PubMed]
11. Nørstrud, H.; Øye, I.J. On CFD simulation of ski jumping. *Comput. Fluid Dyn. Sport Simul.* **2009**, *72*, 63–82.
12. Meile, W.; Reisenberger, E.; Mayer, M.; Schmolzer, B.; Muller, W.; Brenn, G. Aerodynamics of ski jumping: Experiments and CFD simulations. *Exp. Fluids* **2006**, *41*, 949–964. [CrossRef]
13. Virmavirta, M.; Isolehto, J.; Komi, P.; Schwameder, H.; Pigozzi, F.; Massazza, G. Take-off analysis of the Olympic ski jumping competition (HS-106 m). *J. Biomech.* **2009**, *42*, 1095–1101. [CrossRef]
14. Virmavirta, M.; Komi, P.V. Measurements of the take-off forces in ski-jumping Part I and II. *Scand. J. Med. Sci. Sports* **1993**, *3*, 229–243. [CrossRef]
15. Virmavirta, M.; Kivekas, J.; Komi, P.V. Take-off aerodynamics in ski jumping. *J. Biomech.* **2001**, *34*, 465–470. [CrossRef]
16. Virmavirta, M. Ski Jumping: Aerodynamics and Kinematics of Take-Off and Flight. In *Handbook of Human Motion*, 1st ed.; Springer: New York, NY, USA, 2017; pp. 1–21.
17. Virmavirta, M.; Kivekas, J.; Komi, P.V. Ski jumping take-off in a wind tunnel with skis. *J. Appl. Biomech.* **2011**, *27*, 375–379. [CrossRef]
18. Muller, W. Performance factors in ski jumping. *J. Biomech.* **2006**, *39*, 192–213. [CrossRef]
19. Wang, Z.X.; Li, R.; Guan, Z.H.; Wu, D.Y. Experimental study on the initial attitude during Flight in Ski Jumping. *China Sport Sci.* **1998**, *18*, 121–124.
20. Zhang, D.; Zou, X.S.; Liu, Y.; Xu, J.C.; Cao, C.M. Effects of Movement and Postures on Aerodynamic Drag during Ski Jumping In-Run and Take-off Phases in Nordic Combined Athletes. *China Sport Sci. Technol.* **2023**, *59*, 3–12.

21. Tan, X.N.; Zhou, Y.; Qu, F.; Huo, B.; Fu, Y.; Jiang, L. Analysis of Take-off Factors Affecting the Flying Distance of Chinese Elite Male Ski Jumpers. *China Sport Sci. Technol.* **2022**, *58*, 38–45.
22. Cao, F.R.; Wu, X.; Tang, W.D.; Suo, X.; Yang, C.H.; Liu, Y. A systematic review of research on the biomechanics of take-off and early flight of ski jumping. *J. Beijing Univ. Sport.* **2022**, *45*, 35–44.
23. Liu, J.T.; Zuo, Z.G.; Liu, S.H.; Wu, Y.L.; Wang, L.Q. A nonlinear partially-averaged Namer-Stokes model for turbulence flow simulations. *J. Drain. Irrig. Mach. Eng.* **2015**, *33*, 572–576.
24. Keizo, Y.; Makoto, T.; Jun, I.; Keiji, O.; Sophie, B. Effect of posture on the aerodynamic characteristics during take-off in ski jumping. *J. Biomech.* **2016**, *49*, 3688–3696.
25. Schmolzer, B.; Muller, W. The importance of being light: Aerodynamic forces and weight in ski jumping. *J. Biomech.* **2002**, *36*, 1059–1069. [CrossRef] [PubMed]
26. Schwameder, H. Biomechanics research in ski jumping: 1991–2006. *Sports Biomech.* **2008**, *7*, 114–136. [CrossRef]